Structure and dynamics of the negative-ion resonance in H_2, D_2, and HD at 10 eV

Suvasis Swain,[1] E. Krishnakumar,[2] and Vaibhav S. Prabhudesai[1,*]
[1]*Tata Institute of Fundamental Research, Mumbai 400005, India*
[2]*Raman Research Institute, Bengaluru 560080, India*

(Received 12 November 2020; accepted 20 May 2021; published 4 June 2021)

The angular distribution of the anions formed in the dissociative electron attachment (DEA) to H_2, D_2, and HD is studied for the 10-eV resonance using the velocity slice imaging technique. The angular distributions of H^- and D^- from HD are found to be identical and very similar to that of H^- (D^-) from H_2 (D_2) indicating that the distinct dissociation limits for H^- and D^- channels and the small but finite dipole moment of HD do not affect the DEA process. The angular distributions suggest that the main contribution for this resonance is from the capture of s and d partial waves of the attaching electron confirming the resonance to be a $^2\Sigma_g^+$ state. The relative amplitudes of the two partial waves as a function of electron energy also indicate the contribution from a higher-lying $^2\Sigma_g^+$ state through possible predissociation at higher electron energies.

DOI: 10.1103/PhysRevA.103.062804

I. INTRODUCTION

Dissociative electron attachment (DEA) to a molecule gives us a wealth of information in understanding various negative ion states of the molecule. In this process, a free electron is resonantly attached to the molecule to form a temporary negative ion, which dissociates to form an anion and one or more neutral fragments. Though DEA studies are more than half a century old, new insights into this process are still emerging, such as the observation of single-electron attachment leading to the creation of a coherent superposition of two resonances of opposite parity in H_2 and D_2 [1]. This has been made possible by the recent developments in negative ion momentum imaging in low energy electron collision studies [2]. The observation of the quantum coherence in DEA to H_2 and D_2 [1] has also highlighted the limited knowledge that exists on the simplest molecular negative ion states.

DEA to H_2 not only has importance in understanding the fundamental physics of electron molecule collisions but also finds relevance in the processes that are important in the astrophysical environment as well as in plasma processes. Associative detachment, which is the reverse process of DEA, is considered to be an important mechanism in the formation of H_2 leading to the formation of first-generation stars [3] and a source of H_2 in the interstellar medium [4]. DEA to H_2 also helps in the development of ion sources [5] as well as in the fusion edge plasmas [6].

In the low energy ($<$17 eV) electron interaction with H_2, DEA is the only mode of production of hydride negative ion (H^-), crucial in the chemistry of interstellar medium as well as in the fusion plasmas. A large number of studies have been carried out experimentally as well as theoretically on electron attachment to H_2 and its isotopologues over the last few decades [7–26]. The DEA cross section shows peaks mainly [20] at 4, 10, and 14 eV. It is well established that the 4-eV peak in the ion yield curve is due to the lowest attractive $X^2\Sigma_u^+$ anion ground state that dissociates into H (^2S) and $H^-(^1S)$. The 14-eV peak is found to be due to the coherent excitation of both $^2\Sigma_g^+$ and $^2\Sigma_u^+$ anion states that dissociate to $H(2, l)$ and H^- (1^S) [2]. In addition to the three main peaks, signatures of resonances leading to the formation of H^- along with H in higher principal quantum numbers ($n > 2$) close to the polar dissociation threshold have been reported [21]. The second broad peak extending from 6 to 13 eV with a maximum at 10 eV has been identified as due to the repulsive $B\,^2\Sigma_g^+$ negative ion state that dissociates to the lowest limit of $H(^2S) + H^-(^1S)$ which is at ∼3.8 eV w.r.t the vibrational ground state of the neutral molecule. Hence, the total kinetic energy of the two fragments formed from this resonance is considerably high ranging from 2.2 eV at 6 eV to 9.2 eV at 13 eV electron energy. As discussed later, this high kinetic energy release poses experimental challenges in studying this resonance.

This broad resonance around 10 eV has been studied quite extensively using theoretical methods with considerable attention to its nature. While the symmetry of this resonance has been confirmed as $^2\Sigma_g^+$, there has been a discussion about whether it is a Feshbach or a shape resonance. The initial calculations of Bardsley *et al.* [9] found this resonance to lie above the parent $b^3\Sigma_u^+$ neutral state from 1 to 6 atomic units implying that it is a shape resonance. Similar findings have been reported by Buckley and Bottcher with the Feshbach projection-operator calculations, Bardsley and Cohen with the variational calculations, and Bardsley and Wadehra with the *ab initio* resonant scattering calculations with the fits to the experimental data [14,16,17]. They all reported that the $B^2\Sigma_g^+$ resonance is of shape resonance nature up to 5.25 a.u. of internuclear separation. Bardsley and Wadehra [17] also reported possible decay to the parent $b^3\Sigma_u^+$ state by electron ejection. Eliezer *et al.* [11] carried out *ab initio* calculations using the quasivariational method and found that the potential energy curve of the resonance crossing the parent

*vaibhav@tifr.res.in

state $b^3\Sigma_u^+$ approximately in the middle of the Franck-Condon region. This implied that the nature of the resonance changes from a shape to valence excited Feshbach resonance when the internuclear separation increases beyond 1.5 a.u. Using a semiempirical method and incorporating the isotope effect of the DEA cross sections, Chen and Peacher [12] obtained results very similar to that by Eliezer *et al.* [11]. They found the resonance curve intersecting the neutral curve in the middle of the Franck-Condon region and undergoing a corresponding change from shape resonance to Feshbach resonance above 1.5 a.u. of internuclear separation. In terms of energy, this implied that above 9.5 eV it is a shape resonance and below 9.5 eV it is a Feshbach resonance. The most extensive calculations of the electron-H_2 scattering have been by Stibbe and Tennyson [18]. They used the R-matrix method and found that the potential energy curve of this particular resonance lies below the $b^3\Sigma_u^+$ neutral state for internuclear separations less than 1.1 a.u. (above 13.3 eV) only, thus giving it a shape resonance character in the entire Franck-Condon region (1.2 to 1.65 a.u.) with its width varying from 2.2 eV at $2a_0$ to 0.47 eV at $4a_0$. These calculations have remained as a benchmark, based on which several aspects of the resonances have been studied in more detail [23–26].

On the experimental front, this resonance has been studied extensively in terms of electron spectroscopy as well as DEA. Most of the electron spectroscopy work related to resonant interaction has been carried out several decades back and has been reviewed [27]. Later compilations include the assessment of various electron scattering data on H_2, D_2, and HD [28,29], and a recent report [30] on excitation of the $b^3\Sigma_u^+$ state. There are a few other publications that have mostly dealt with DEA. Absolute DEA cross sections were reported by Schulz [7], Rapp *et al.* [8], and Krishnakumar *et al.* [20]. Rapp *et al.* and Krishnakumar *et al.* have measured the isotope effects on the absolute cross sections as well. Dowel and Sharp [13] reported the vibrational structure starting from 11.2 eV on the H^- ion yield curve. Tronc *et al.* [15] were able to reproduce this though such structures were not observed either by Dowel and Sharp or Tronc *et al.* for D_2. In addition, Tronc *et al.* [15] carried out measurements of the angular distribution of H^- from H_2 for this resonance and identified its symmetry to be $^2\Sigma_g^+$. An interesting aspect of electron scattering work on this resonance that has not received much attention so far is the signature of quantum interference between the ground $X^2\Sigma_u^+$ state and the $B\,^2\Sigma_g^+$ state observed in the vibrational excitation of the ground state of H_2 by Hall and Andric [31]. The $X\,^2\Sigma_u^+$ state responsible for the 4 eV peak in DEA could energetically overlap with the $B\,^2\Sigma_g^+$ state due to its large width (∼10 eV) and thus give rise to the observed interference. Considering this and in the context of the observation of coherent excitation of resonances at 14 eV [1], we felt it worthwhile to investigate the angular distribution for the 10 eV resonance. Moreover, there are no reports on the angular distribution of ions from DEA to HD, which strictly is not a homonuclear diatomic molecule. In this work, we report a detailed study of the angular distribution of H_2 and its two isotopologues D_2 and HD using the velocity slice imaging technique, which can provide the angular distribution over the entire 2π angular range, in comparison to previous measurements [15].

II. EXPERIMENT

The measurements are carried out using a momentum imaging time of flight (TOF) spectrometer, which has been described earlier [2,32]. For completeness, a brief description is as follows. A magnetically collimated electron beam pulse of 100 ns duration is made to interact with an effusive molecular beam at room temperature produced by a capillary array. The anions formed in the interaction region are then extracted into a velocity map imaging TOF spectrometer using a pulsed electric field (50-V amplitude and 1-μs width) with a delay of 100 ns after the electron pulse. The ions are detected using a two-dimensional position-sensitive detector (PSD) comprising of a pair of microchannel plates in the chevron geometry followed by a phosphor screen. The image on the phosphor screen is recorded using a charge-coupled device camera. Velocity slice images (VSIs) are taken by applying a pulsed bias of the detector simultaneous with the arrival of the central slice of the Newton sphere of the relevant ions. In the present experiment, the width of the biasing pulse of the detector is kept as 80 ns. The VSIs so obtained are then analyzed after adding several such slices in the offline analysis.

Momentum imaging of H^- ions produced from the 10-eV resonance is particularly challenging due to their low mass and high kinetic energies (∼4 eV for H_2 and ∼5.3 eV for HD at an electron energy of 12 eV). The low mass and high kinetic energy necessitate the use of a relatively small duration electron beam pulse to limit the spread of ions in the interaction region before the ion extraction field is turned on. This has an undue consequence on the electron energy resolution making it about 0.8 eV full width at half maximum in the present case. The low mass and high kinetic energy also affect the momentum imaging due to the presence of the magnetic field used for collimating the electron beam. The field is produced by a pair of Helmholtz coils mounted outside the vacuum chamber. The magnetic field causes a deviation in the trajectories of the ions causing them to be asymmetric about the axis of the ion spectrometer and consequently making some of the trajectories pass close to the electrostatic lens apertures. This distorts the image as well as causes loss of ions. This effect becomes more prominent with higher energy ions. We addressed this problem by using a smaller flight tube and larger apertures. The smaller flight tube reduces the mass resolution of the spectrometer. However, we have found the operating conditions of the spectrometer with good enough mass resolution to separate H^- and D^- ions. We have optimized the extraction field and the spectrometer biases with utmost care for imaging the energetic H^- ions produced across the broad resonance around 10 eV. Despite these best efforts, we still faced problems in imaging very high kinetic energy H^- ions, as discussed below. However, the cylindrical symmetry about the electron beam and the fact that molecules in the target beam have no preferred orientation allowed us to overcome this by analyzing only one-half of the images.

Due to the low DEA cross section, we had to operate the spectrometer at 3×10^{-6} torr background pressure to obtain sufficient statistics in a reasonable time. Such a high background pressure was found to give considerable distortion in the momentum images. We found that this was due to the substantial contribution of the H^- ions from the static gas

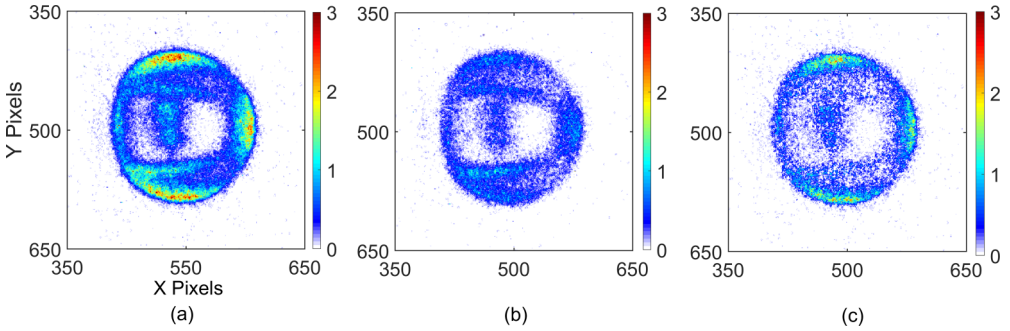

FIG. 1. Momentum image of H^- from H_2 obtained at 10 eV by (a) crossed beams geometry where the contributions from background gas and the molecular beam are present, (b) static gas geometry where the only contribution from the background gas is present, and (c) subtracting the one in (b) from that in (a) giving only the contribution from the molecular beam. The direction of the electron beam is from top to bottom.

background as compared to the molecular beam signal. The static gas background produced an extended source of ions over and above the pointlike source that the overlap of the electron beam and the molecular beam normally creates. This unwanted source of ions gave rise to additional features in the momentum images as shown in Fig. 1(a). Figure 1(b) shows the static gas contribution to the image. This is obtained by diverting the gas flow into the chamber through another entrance instead of the capillary used to make the effusive beam while keeping the background pressure the same. On the subtraction of the static gas image [Fig. 1(b)] from the molecular beam plus static gas image [Fig. 1(a)] (after due normalization for any variation of the integrated electron beam current and pressure), we get the image in Fig. 1(c). Considering the relatively low cross sections and the need to build good enough statistics, the measurements are carried out for fairly long durations. As can be seen from Fig. 1(c), most of the static gas contribution has been removed using this subtraction procedure. This procedure has been used in all the images that we obtained for the present study.

We can also see that the images are heavily distorted on their left side. As discussed above, this is due to the magnetic field used for collimating the electron beam. The effect of the transverse magnetic field is to shift the entire Newton sphere to one side of the VMI spectrometer axis due to the $v \times B$ force where v is the velocity of the ions which has a major component along the spectrometer axis and B is the magnetic field. This shift brings one side of the Newton sphere closer to the edge of the VMI electrode apertures distorting the imaging. Larger-sized Newton spheres could even get chopped at one side depending on the $v \times B$ force. However, azimuthal symmetry about the electron beam allows us to overcome this problem by using only the right half of the image which is obtained near the center of the detector for analysis.

III. RESULTS AND DISCUSSION

We have obtained VSIs of H^- (D^-) produced from H_2 (D_2) and both H^- and D^- from HD at electron energies ranging from 8.5 to 12 eV at 0.5 eV interval. The VSIs are then converted into momentum images.

The momentum images obtained at 10 eV for both H^-/H_2 and D^-/D_2 are shown in Fig. 2. As can be seen from the image, the electron energy uncertainty shows up as a spread in the ion image along the radial direction. The blob seen in the center of the image is due to the long energy tail of the electron beam which produces negative ions from the 14 eV resonance. Since these ions have very low kinetic energy, all the ions emitted in the entire 4π solid angle are detected in the slice of the Newton sphere in comparison to the ions from the 10 eV resonance, thus giving it an undue weightage. The observed shift of this blob away from the center of the image is a consequence of the electron-beam-collimating magnetic field which is transverse to the direction of the ion spectrometer. This is consistent with the SIMION simulations we carried out. We have obtained the angular distribution for given electron energy by analyzing the momentum image in a restricted annular region. This annular region is selected to be as close to the edge of the image as possible which will give reasonable statistics. We limit the annular region to compensate for the relatively poor electron energy resolution in the present case, as there is only one dissociation limit relevant for the electron energy range giving one to one correspondence between the electron energy and kinetic energy of the ions. The electron beam energy was calibrated using the 14-eV peak in the H^-/H_2 as well as from the rising edge of the O^-/CO. As mentioned above, to avoid the effect of the transverse magnetic field only the right half of the image is used to obtain the angular distribution.

The measured angular distribution from H_2, D_2 along with that reported by Tronc *et al.* for H_2 [15] are shown in Fig. 3 for 10-eV electron energy. It is expected that the angular distribution obtained from the same resonant state should not

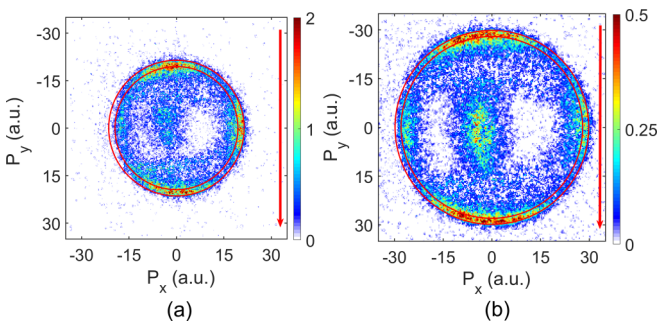

FIG. 2. Momentum image obtained for (a) H^- from H_2 and (b) D^- from D_2 at 10 eV of electron energy. The incident electron beam direction is from top to bottom as indicated by the arrow in the image.

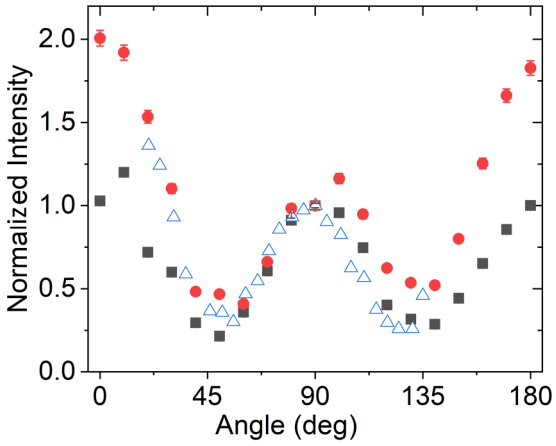

FIG. 3. Comparison of the angular distribution of (■) H^-/H_2 and (●) D^-/D_2 in the present measurements at 10 eV electron energy with the earlier reported (Δ) H^-/H_2 data by Tronc *et al.* [15].

change from H_2 and D_2 since the orientation dependence of the electron attachment cross section does not depend on the change in their mass. In general, the present angular distribution is in fair agreement with the existing data, confirming the $^2\Sigma_g^+$ symmetry of the resonance. One may note from Fig. 3 that the distribution obtained for D_2 matches better with that of H_2 measured by Tronc *et al.* [15]. We attribute this to the poorer imaging of the faster moving H^- as compared to D^-. The larger mass of D^- causes it to have a relatively smaller magnetic field-induced deviation of its trajectories and a smaller spatial spread in the ionizing region before the ion extraction field is turned on improving its velocity focusing. Moreover, the spread in the TOF for D^- is larger than that for H^- making the fixed-width slicing more accurate for the former.

For HD, the H^- channel has double the kinetic energy than the D^- channel due to linear momentum conservation. As a result, it is even more difficult to obtain the velocity slice image of this channel. We have obtained the partial image for this channel and the complete image of the D^- channel. The images and the corresponding angular distributions for both channels at 10-eV electron energy are shown in Figs. 4 and 5 respectively. The angular distributions for both ions are almost identical and similar to those observed in H_2 and D_2. The dissociation limits for both H^- and D^- channels differ

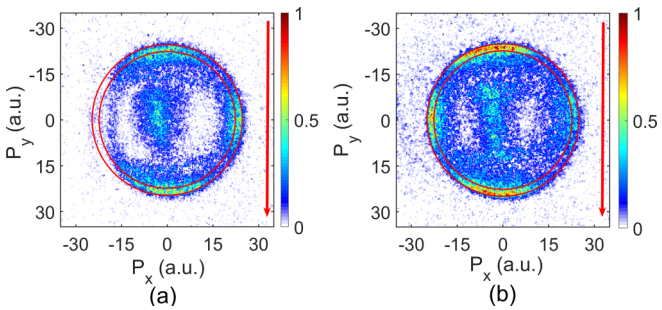

FIG. 4. Momentum image obtained for (a) H^- and (b) D^- from HD at 10 eV electron energy. The electron beam is from top to bottom as indicated by the arrow marked in the image.

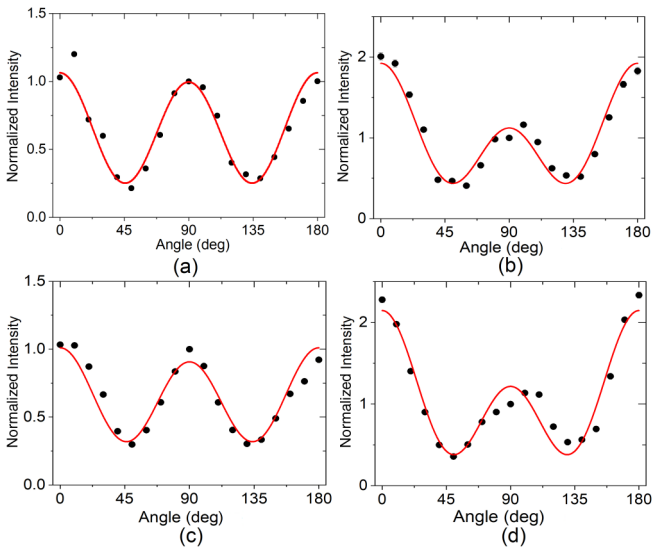

FIG. 5. Measured angular distribution for fragment ions from (a) H_2, (b) D_2, (c) H^- from HD, and (d) D^- from HD at 10 eV electron energy. The data are normalized at 90° about the electron beam direction. Measured data is represented by the filled circles and the fitted distribution is represented by a solid line (see the text).

by 400 μeV due to the difference in the electron affinity of the H and D [33]. It has been shown that incorporating the mass effects in the molecular wave function makes HD a heteronuclear diatomic molecule particularly close to the dissociation limit. This is a consequence of the mass-dependent terms, which are otherwise neglected in the Hamiltonian to get the Born-Oppenheimer approximation, coming into play and mixing the states with opposite parity [34]. In the present case, the two dissociation limits namely $H^- + D$ and $D^- + H$ can be understood to be arising from the mixing of $X\ ^2\Sigma_u^+$ and $B\ ^2\Sigma_g^+$ state with one being $\frac{1}{\sqrt{2}}(X^2\Sigma_u^+ + B^2\Sigma_g^+)$ and the other being $\frac{1}{\sqrt{2}}(X^2\Sigma_u^+ - B^2\Sigma_g^+)$.

Under the axial recoil approximation [35] where the dissociating bond is assumed to maintain its orientation with respect to the electron beam, the observed angular distribution of the DEA process will entirely depend on the structure of the initial neutral state and the final anion resonant state resulting from the electron capture. In this case, there is only one resonance from the Franck-Condon region which is contributing to the DEA signal in the 10-eV peak. In the DEA to HD across the 10-eV peak both the channels ($H^- + D$ and $D^- + H$) result from this resonance. This explains the identical angular distribution observed for both channels. Moreover, as these angular distributions are similar to the ones obtained from both H_2 and D_2, we can conclude that the permanent dipole moment arising from the asymmetric mass of HD does not play any significant role in the electron capture. In other words, HD seems to behave like a homonuclear diatom for the electron capture process.

For a homonuclear diatomic molecule, due to the inversion symmetry present in the system, the electron attachment must proceed through the transfer of only odd or only even partial waves to the target molecule [35]. The angular distribution is

then given by

$$I(k,\theta,\varphi) = \left|\sum_{l=m}^{\infty} A_{lm}(k) Y_{lm}(\theta,\varphi)\right|^2,$$

where A_{lm} is the transition amplitude, l is the orbital angular momentum of the incident electron, m is the difference in electronic axial orbital angular momenta of the target state and resonant state of the molecule, and Y_{lm} is the spherical harmonic [36]. Here the angle θ represents the angle of ejection of the fragment with respect to the incoming electron beam in the laboratory frame.

As both the target neutral state of H_2 ($X\ ^1\Sigma_g^+$) and the resonant state of H_2^- ($B^2\Sigma_g^+$) have even parity, the transition is possible by the capture of only even partial waves. This implies that l will take only even values. To see any contribution from the lower $X\ ^2\Sigma_u^+$ state in the DEA around 10 eV, we looked for possible forward-backward asymmetry that would arise from the quantum interference of the p wave (necessary for the formation of $X\ ^2\Sigma_u^+$ resonance) and s and d waves (giving rise to the $B\ ^2\Sigma_g^+$ resonance). Within the uncertainties of the measurements, we could not observe any asymmetry in any of the angular distributions we investigated here. This is not surprising since even if the $X\ ^2\Sigma_u^+$ resonance is initially formed it has very little probability to survive long enough to contribute to the DEA channel at this range of energy, due to its very short autodetachment lifetime.

Tronc *et al.* [15] have crudely evaluated the limit of l values that could contribute to the DEA process for this resonance by approximating the dimension of the electron cloud in the resonant state. Based on that, they have found the contribution up to $l = 2$ is important and the contribution above that is very small and can be neglected. Hence, the angular distribution function takes the form

$$I(k,\ \theta,\varphi) = \left|A_{0,0}(k)Y_{0,0}(\theta,\varphi) + e^{i\delta}A_{2,0}(k)Y_{2,0}(\theta,\varphi)\right|^2.$$

Taking into account the azimuthal symmetry of the process and applying the axial recoil approximation, the functional form of the expected angular distribution of the H^- fragment is given by

$$I(k,\theta) = \frac{A_{0,0}^2}{4\pi} + 5\frac{A_{2,0}^2}{16\pi}(3\cos^2\theta - 1)^2 + \sqrt{5}\frac{A_{0,0}A_{2,0}}{4\pi}(3\cos^2\theta - 1)\cos\delta,$$

where $A_{0,0}$ and $A_{2,0}$ are transition amplitudes corresponding to the attachment of the $l = 0$ (s wave) and $l = 2$ (d wave) partial waves of the attaching electron, respectively, δ is the relative phase between the two partial waves. The measured angular distributions are fitted for the above functional form. The data at 10 eV along with the fits are given in Fig. 5 to show the consistency of the fits. The values of the transition amplitudes, as well as the relative phases for different incident electron energies obtained from the fits, are given in Table I.

It can be seen from the Table that for up to 10-eV electron energy, the amplitudes for both the partial waves are nearly the same. This is consistent with the earlier reported results [15]. We also note that beyond 10 eV, the amplitude of d wave decreases substantially whereas the amplitude of s wave increases with an increase in incident electron energy. This behavior is seen in all four cases. For ease of comparison, we plot the ratio of the amplitudes of the two waves in Fig. 6. From the figure, we can see that except for the 8-eV data of H^- from HD, the rest show a consistent behavior. The ratio is almost constant up to 10.5 eV and starts increasing with energy at higher energies showing the increasing contribution of s wave as compared to the d wave. The previous measurements by Tronc *et al.* [15] on H_2 also reported a variation of the relative amplitudes of the two waves in a similar way as shown in Fig. 6.

Tronc *et al.* [15] interpreted the increase in the s-wave amplitude as due to the additional contribution from the second resonance of identical symmetry. The ion yield measurements of H^- from H_2 have shown the possibility of predissociation from a second ($^2\Sigma_g^+$) resonance contributing to the DEA process from 11 eV onwards in terms of the discrete structure overlapping the cross section [13,15], though the fact that such structure was not seen in the case of D_2 remains as an enigma. We looked for the signatures of these discrete structures in our momentum images since the electron energy spread in our experiment is about 800 meV. Any structure, if present, should manifest as structures in the momentum images, assuming the momentum imaging resolution of the spectrometer is not a limiting factor. We could not reproduce the oscillations observed in the data reported by Tronc *et al.* [15] in a given image. This may be due to insufficient momentum imaging resolution of the present measurements because of the slicing width of 80 nsec and comparatively limited spread of the TOF spectrum of the H^- ions. In terms of kinetic energy, we

TABLE I. Relative amplitudes and phase from the angular distribution fit of H^- from H_2 and D^- from D_2.

	H_2			D_2		
e-Energy (eV)	A_{00}	A_{20}	δ(rad)	A_{00}	A_{20}	δ(rad)
8.5	2.38 ± 0.18	2.17 ± 0.13	1.89 ± 0.08	2.39 ± 0.15	2.29 ± 0.1	1.83 ± 0.06
9	2.08 ± 0.14	2.16 ± 0.08	1.99 ± 0.06	2.3 ± 0.11	2.27 ± 0.07	1.72 ± 0.04
9.5	2.1 ± 0.16	2.09 ± 0.1	1.97 ± 0.07	2.17 ± 0.1	2.17 ± 0.06	1.81 ± 0.04
10	2.03 ± 0.1	1.86 ± 0.07	2.06 ± 0.05	2.4 ± 0.12	2.16 ± 0.08	1.78 ± 0.05
10.5	2.14 ± 0.08	1.72 ± 0.06	2.03 ± 0.04	2.22 ± 0.09	1.91 ± 0.07	1.82 ± 0.04
11	2.47 ± 0.07	1.43 ± 0.07	2.04 ± 0.03	2.52 ± 0.08	1.86 ± 0.06	1.83 ± 0.03
11.5	2.48 ± 0.05	1.28 ± 0.06	2.15 ± 0.03	2.61 ± 0.07	1.54 ± 0.07	1.9 ± 0.03
12	2.61 ± 0.06	1.03 ± 0.1	2.1 ± 0.03	–	–	–

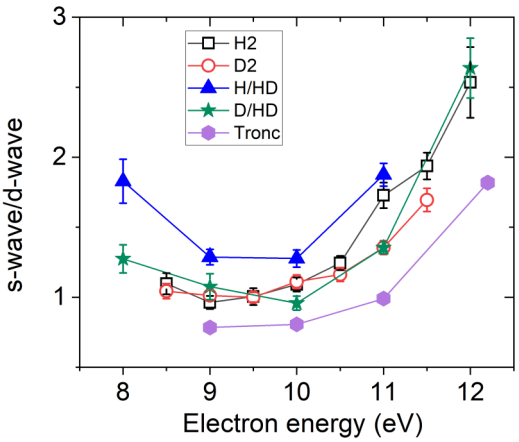

FIG. 6. Ratio of the amplitude of s-wave to that of d-wave capture obtained from the fit to the angular distribution of (□) H^- from H_2, (◯) D^- from D_2, (▲) H^-, and (★) D^- from HD as a function of electron energy. The filled hexagons (⬢) are the data from Tronc *et al.* [15].

estimate the resolution to be about 300 meV at the observed kinetic energy of the ions. This may not have been good enough to observe the oscillations of similar width due to overlap of the thicker slice of the Newton sphere. Hence we do not rule out the contribution from the higher $^2\Sigma_g^+$ resonance and go with the interpretation of Tronc *et al.* [15] regarding the observed change in the ratio of the two partial waves.

There exist a set of results from electron scattering experiments relevant to the discussion on these two $^2\Sigma_g^+$ resonances. The presence of the $C\,^2\Sigma_g^+$ resonance with discrete vibrational levels has been observed in the electron scattering channel [38], consistent with the structure observed in the ion yield curve of Tronc *et al.* [15]. However, it appears that there is some inconsistency between the electron scattering data and theoretical calculations regarding the lower $B\,^2\Sigma_g^+$ resonance. As mentioned in the introduction, the theoretical calculations have shown that the $B\,^2\Sigma_g^+$ resonance crosses the parent $b\,^3\Sigma_u^+$ state although most of the calculations have shown that across the Franck-Condon region the resonance lies above the parent state and may decay to the parent state. The curve crossing has been estimated to be around 13.3 eV by Stibbe and Tennyson and concluded that below this energy the resonance predominantly decays to the parent $b^3\Sigma_u{}^+$ state [18]. The observation of a 0.8-eV shift in the collisional detachment signal in the H^- and D reaction has been treated as the direct evidence of the shape resonance nature of this resonance [37]. This is in agreement with the understanding that for internuclear separation larger than 1.7 a. u. and extending up to reasonably large separation the shape resonance character exists. There exists no signature of resonant excitation of $b^3\Sigma_u^+$ state through the $B\,^2\Sigma_g^+$ resonance for electron energies above 10.5 eV in the available electron scattering data. This is seen from the data of Weingartshofer *et al.* [38] where the scattered electron yield with energy loss of 10.47 eV shows only a direct scattering-type feature in the $b\,^3\Sigma_u^+$ excitation that peaks at 11.5 eV. The only resonance feature observed in their spectrum was due to vibrational levels of the higher bound $C^2\Sigma_g^+$ resonance that contributes from 11.2 eV onwards [38]. Hall and Andric [31] have shown that the angular distribution of the scattered electron from upwards of 10.5 eV leading to excitation of $b\,^3\Sigma_u^+$ is consistent with that expected from the direct scattering only. They have also shown that the $b\,^3\Sigma_u^+$ excitation spectrum decreases beyond 10.5 eV whereas the DEA ion yield does not decrease as rapidly. Thus these observations indicate that the resonance curve lies below its parent state above 10.5 eV of electron energy. This shift may be a result of the avoided curve crossing between the two $^2\Sigma_g^+$ states which appear to be contributing together to the DEA process at these energies. We wish to point out that the inconsistency between the electron scattering data [31,38] and the latest theoretical calculations on the potential energy curve of the lower $B^2\Sigma_g^+$ state is yet to be resolved.

IV. SUMMARY AND CONCLUSION

We have studied the role of $B\,^2\Sigma_g^+$ resonance in the DEA to H_2 and its isotopologue D_2 and HD around 10-eV electron energy in terms of the angular distribution of the fragment anion using the velocity slice imaging method. The main contribution to this resonance is due to the transfer of *s* and *d*-partial waves of the attaching electron to the target molecule. As against the quantum interference between the anion ground state and this resonance observed in the electron scattering channel at this energy, we do not see any such signature in the DEA. The angular distribution of the DEA fragments from both H_2 and D_2 shows the contribution from the higher $C^2\Sigma_g^+$ state from 11 eV onwards. Based on the earlier reported electron scattering results we propose that from 10.5 eV onwards the $B^2\Sigma_g{}^+$ resonance lies below the parent $b^3\Sigma_u{}^+$ state which is in contrast with the latest theoretical calculations. In the case of HD, both the H^- and D^- channels show identical angular distributions that match with the one obtained for the homonuclear isotopologues. Hence, we conclude that HD behaves like a homonuclear diatom in the electron attachment process and its permanent dipole moment does not have any noticeable effect on the electron capture process and hence the DEA process.

ACKNOWLEDGMENTS

E.K. acknowledges the Raja Ramanna Fellowship from the Department of Atomic Energy, India. S.S. and V.S.P. acknowledge the financial support from the Department of Atomic Energy, India under the Project Identification No. RTI4002.

[1] E. Krishnakumar, Vaibhav S. Prabhudesai, and Nigel J. Mason, Nat. Phys. **14**, 149 (2018).
[2] D. Nandi, V. S. Prabhudesai, A. Chatterjee, and E. Krishnakumar, Rev. Sci. Instrum. **76**, 053107 (2005).
[3] H. Kreckel, H. Bruhns, M. Cizek, S. C. O. Glover, K. A. Miller, X. Urbain, and D. W. Savin, Science **329**, 69 (2010).
[4] D. Field, Astron. Astrophys. **362**, 774 (2000).
[5] M. Bacal, Nucl. Fusion **46**, S250 (2006).

[6] M. Bacal and M. Wada, App. Phys. Rev. **2**, 021305 (2015).
[7] G. J. Schulz, Phys. Rev. **113**, 816 (1959).
[8] D. Rapp, T. E. Sharp, and D. D. Briglia, Phys. Rev. Lett. **14**, 533 (1965).
[9] J. N. Bardsley, A. Herzenberg, and F. Mandl, Proc. Phys. Soc. **89**, 305 (1966).
[10] G. J. Schulz and R. K. Asundi, Phys. Rev. **158**, 25 (1967).
[11] I. Eliezer, H. S. Taylor, and James Williams, J. Chem. Phys. **47**, 2165 (1967).
[12] Joseph C. Y. Chen and Kerry L. Peacher, Phys. Rev. **167**, 30 (1968).
[13] J. T. Dowel and T. E. Sharp, Phys. Rev. **167**, 124 (1968).
[14] Brian D. Buckley and Christopher Bottcher, J. Phys. B **10**, L635 (1976).
[15] M. Tronc, F. Fiquet-Fayard, C. Schermann, and R. I. Hall, J. Phys. B **10**, 305 (1977).
[16] J. N. Bardsley and J. S. Cohen, J. Phys. B **11**, 3645 (1978).
[17] J. N. Bardsley and J. M. Wadehra, Phys. Rev. A **20**, 1398 (1979).
[18] Darian T. Stibbe and Jonathan Tennyson, J. Phys. B **31**, 815 (1998).
[19] H. Drexel, G. Senn, T. Fiegele, P. Scheier, A. Stamatovic, N. J. Mason, and T. D. Märk, J. Phys. B Opt. Phys. **34**, 1415 (2001).
[20] E. Krishnakumar, S. Denifl, I. Čadež, S. Markelj, and N. J. Mason, Phys. Rev. Lett. **106**, 243201 (2011).
[21] I. Čadež, R. I. Hall, M. Landau, F. Pichou, M. Winter, and C. Schermann, Acta Chim. Slov. **51**, 11 (2004).
[22] E. M. de Oliveira, M. A. P. Lima, and M. T. do N. Varella, Phys. Rev. A **78**, 042704 (2008).
[23] R. Celiberto, R. K. Janev, J. M. Wadehra, and A. Laricchiuta, Phys. Rev. A **77**, 012714 (2008).
[24] R. Celiberto, R. K. Janev, J. M. Wadehra, and A. Laricchiuta, Phys. Rev. A **80**, 012712 (2009).
[25] R. Celiberto, R. K. Janev, J. M. Wadehra, and J. Tennyson, Chem. Phys. **398**, 206 (2012).
[26] R. Celiberto, R. K. Janev, V. Laporta, J. Tennyson, and J. M. Wadehra, Phys. Rev. A **88**, 062701 (2013).
[27] G. J. Schulz, Rev. Mod. Phys. **45**, 423 (1973).
[28] Jung-Sik Yoon, Mi-Young Song, Jeong-Min Han, Sung Ha Hwang, Won-Seok Chang, BongJu Lee, and Yukikazu Itikawa, J. Phys. Chem. Ref. Data **37**, 913 (2008).
[29] Jung-Sik Yoon, Young-Woo Kim, Deuk-Chul Kwon, Mi-Young Song, Won-Seok Chang, Chang-Geun Kim, Vijay Kumar, and BongJu Lee, Rep. Prog. Phys. **73**, 116401 (2010).
[30] M. Zawadzki, R. Wright, G. Dolmat, M. F. Martin, B. Diaz, L. Hargreaves, D. Coleman, D. V. Fursa, M. C. Zammit, L. H. Scarlett, J. K. Tapley, J. S. Savage, I. Bray, and M. A. Khakoo, Phy. Rev. A **98**, 062704 (2018).
[31] R. I. Hall and L. Andric, J. Phys. B **17**, 3815 (1984).
[32] K. Gope, V. Tadsare, V. S. Prabhudesai, and E. Krishnakumar, Euro. Phys. J. D **71**, 323017 (2017).
[33] NIST Chemistry Webbook: https://webbook.nist.gov/chemistry/.
[34] A. De Lange, E. Reinhold, and W. Ubachs, Int. Rev. Phys. Chem. **21**, 257 (2002).
[35] T. F. O'Malley and H. S. Taylor, Phys. Rev. **176**, 207 (1968).
[36] R. J. Van Brunt and L. J. Kieffer, Phys. Rev. A **2**, 1899 (1970).
[37] V. A. Esaulov, J. Phys. B **13**, 4039 (1980).
[38] A. Weingartshofer, H. Ehrhard, V. Hermann, and F. Linder, Phys. Rev. A **2**, 294 (1970).